DOI:
10.1016/j.cmpb.2022.106781

Document Version
Peer reviewed version

This is the Author's Accepted Manuscript version of the article: Yang, Y., Zhou, S., Alastruey, J., Hao, L., Greenwald, S.E., Zang, Y., Xu, L., Xu, L. & Yao, Y. (2022). Estimation of central pulse wave velocity from radial pulse wave analysis. Comp. Meth. Prog. Med. Accepted for publication on 26 March 2022.

Estimation of Central Pulse Wave Velocity from Radial Pulse Wave Analysis

Yang Yao, Shuran Zhou, Jordi Alastruey, Liling Hao, Stephen E. Greenwald, Yuelan Zhang, Lisheng Xu*, *Senior Member, IEEE*, Yudong Yao, *Fellow, IEEE*

***Abstract*— *Goal:* Arterial stiffness, commonly assessed by carotid-femoral pulse wave velocity (cfPWV), is an independent biomarker for cardiovascular disease. The measurement of cfPWV, however, has been considered impractical for routine clinical application. Pulse wave analysis using a single pulse wave measurement in the radial artery is a convenient alternative. This study aims to identify pulse wave features for a more accurate estimation of cfPWV from a single radial pulse wave measurement. *Methods:* From a dataset of 111 subjects, cfPWV was measured and the radial pulse waveform was recorded for 30 seconds twice in succession. Features were extracted from the waveforms in the time and frequency domains, as well as by wave separation analysis. All-possible regressions with bootstrapping, McHenry's select algorithm, and support vector regression were applied to select subsets of the features and to estimate cfPWV. *Results:* The correlation coefficient between the measured and estimated cfPWV was r=0.8, r=0.84, and r=0.8 for all-possible regressions, McHenry's select algorithm, and support vector regression, respectively. The features selected by all-possible regressions are physiologically interpretable. In particular, the amplitude ratio of the diastolic peak to the notch of the radial pulse waveform ($R_{n,d}^{r,P}$) is shown to be correlated with cfPWV. This correlation was further evaluated and found to be independent of wave reflections using a dataset (n=3,325) of simulated pulse waves. *Conclusion:* The proposed method may serve as a convenient alternative for the measurement of cfPWV. $R_{n,d}^{r,P}$ is associated with aortic PWV and this association may not be dependent on wave reflection.**

***Index Terms*—arterial stiffness, pulse wave analysis, pulse wave velocity, wave separation analysis**

I. Introduction

AORTIC stiffness is independently associated with cardiovascular events, target organ damage, and all-cause mortality [1, 2]. When added to standard risk factors (e.g., blood pressure), aortic stiffness improves the prediction of cardiovascular events [3]. Carotid-femoral pulse wave velocity (cfPWV) has been proposed as the noninvasive gold standard for assessing aortic stiffness [4-6]. However, its measurement requires a skilled operator and remains confined to specialized centers. Besides, the carotid-femoral distance is hard to estimate accurately in obese patients. Thus, the measurement of cfPWV is not recommended for routine practice [7].

Pulse wave analysis is an alternative technique to assess arterial stiffness using a single arterial pressure waveform. The augmentation index (AIx) calculated from the radial pulse waveform or the synthetized aortic pulse waveform computed from the radial pulse waveform has been suggested as an index of stiffness [8]. However, several influencing factors (e.g., body height and heart rate) limit its performance [8]. In addition, the calculation of AIx is not reliable enough in some subjects due to the difficulty in determining the second peak of the radial pulse waveform or the inflection point of the aortic pulse waveform. In recent years, wave separation analysis (WSA) based on an approximated flow wave has been used to assess arterial stiffness, by calculating the pulse transit time as the time delay between the forward wave and the backward-traveling reflected wave [9]. However, this delay is determined not only

This work was supported by the National Natural Science Foundation of China under Grants 61773110 and 61701099. This research was also supported by the Shenyang Science and Technology Plan Fund (No. 20-201-4-10), the Member Program of Neusoft Research of Intelligent Healthcare Technology, Co. Ltd. (No. MCMP062002). JA acknowledged support from the British Heart Foundation (PG/15/104/31913), the Cardiovascular MedTech Cooperative at Guy's and St Thomas' NHS Foundation Trust, and the Ministry of Science and Higher Education of the Russian Federation (075-15-2020- 926).

Yang Yao was with the College of Medicine and Biological Information Engineering, Northeastern University, Shenyang, Liaoning 110169, China. Currently, he is with the School of Information Science and Technology, ShanghaiTech University, Shanghai, 201210, China (e-mail: yaoyang1@shanghaitech.edu.cn)

Shuran Zhou is with the College of Medicine and Biological Information Engineering, Northeastern University, Shenyang, Liaoning 110169, China (e-mail: zhoushuranbmie@163.com)

Jordi Alastruey is with the Department of Biomedical Engineering, King's College London, London SE1 7EH, UK and with the World-Class Research Center, "Digital Biodesign and Personalized Healthcare", Sechenov University, Moscow, Russia (e-mail: jordi.alastruey-arimon@kcl.ac.uk)

Liling Hao is with the College of Medicine and Biological Information Engineering, Northeastern University, Shenyang, Liaoning 110169, China (e-mail: haoll@bmie.neu.edu.cn)

Stephen Greenwald is with the Blizard Institute, Barts & The London School of Medicine and Dentistry, Queen Mary University of London, London, United Kingdom (e-mail: s.e.greenwald@qmul.ac.uk)

Yuelan Zhang is with The First Hospital of China Medical University, Shenyang, Liaoning 110122, China (e-mail: zhangzyl3@sina.com)

*Lisheng Xu is with the College of Medicine and Biological Information Engineering of Northeastern University, and Neusoft Research of Intelligent Healthcare Technology, Co. Ltd., Shenyang, Liaoning 110169, China (correspondence; phone: 024-8368-3200; fax: 024-8368-3200; e-mail: xuls@bmie.neu.edu.cn).

Yudong Yao is with the Department of Electrical and Computer Engineering, Stevens Institute of Technology, Hoboken, NJ, USA (yyao@stevens.edu)

by the speed of the pulse but also by the distance it travels, i.e. the effective reflection distance (distance from an aortic measurement site to a notional site from which all distal reflections appear to originate), which is influenced by several factors like the length of the arterial tree and central-to-peripheral arterial stiffness gradient [10].

This study aims to investigate the pulse wave features that allow an accurate estimation of cfPWV from a single pulse wave measurement in the radial artery. We firstly extracted a set of features from the radial and derived aortic pulse waveforms (using a transfer function [11]) and identified those that enable accurate cfPWV estimation. The associations of these identified features with aortic stiffness were further confirmed using a dataset of simulated pulse waves in 3325 virtual subjects.

II. Methods

A. Subjects and Experimental Protocol

This study was approved by the biological and medical ethics committee of Northeastern University, China (No. NEU-EC-2020B017S; date of approval: 2020.11.20). A total of 116 subjects were enrolled, all of whom gave informed consent before the study. Five of them were excluded due to lack of evident feature points (inflection points and/or notch) in the derived aortic pulse waveform, resulting in a set of 111 subjects (61 males and 50 females; age, 43±21 years; height, 168±8 cm; weight, 65±11 kg). Table 1 lists the cardiovascular status of the subjects.

TABLE I
CARDIOVASCULAR STATUS OF THE SUBJECTS

# subjects	Cardiovascular abnormality and/or disease
2	Premature left ventricular contraction
2	Arrhythmia
2	Hypertension
1	Hypothyroidism
1	Arteriosclerosis
1	Abnormal mitral regurgitation
1	Myocardial ischemia
1	Coronary heart disease
1	Cerebral infarction and arteriosclerosis
1	Left ventricular insufficiency and atrial fibrillation
1	Hypertension and arrhythmia
1	Arrhythmia, coronary heart disease, and hypothyroidism
96	No cardiovascular abnormality or disease reported

As shown in Fig. 1, after a 5 min. rest, blood pressure was measured in each subject while seated. Subjects remained in a supine position thereafter. After a further 2 min. rest, right carotid and femoral pulse waveforms were simultaneously recorded twice (for at least 30 sec. each time) using two pulse sensors (MP100, Xinhangxingye Co. Ltd., China). Signals were sampled at 1 kHz with a BL-420S data acquisition system (Chengdu Techman Software Co. Ltd, China). Then the straight-line distance between the right carotid and femoral artery sites was measured with a tape to the nearest half centimeter. Immediately following this, the radial pulse waveform was recorded twice, for 10 sec. each time, using a sphygmomanometer (SphygmoCor, AtCor, Australia; sampling at 128 Hz).

B. Calculation of Pulse Wave Velocity

The carotid and femoral pulse signals were processed by removing the baseline drift and noise via wavelet decomposition. More specifically, the baseline was calculated as the approximation layer of a 10-level 'sym7' wavelet decomposition [12, 13]. The noise was approximated by the detail layer of a 4-level 'db7' wavelet decomposition [12, 13].

In each subject, cfPWV was calculated from each of the two simultaneous recordings of carotid and femoral pulse waveforms as suggested by an expert consensus document [4, 5]. For each cardiac period, the respective feet of the carotid and femoral pulse signals were determined by the intersecting tangent method [14, 15]. The carotid-femoral pulse transit time was taken as the time difference between the feet of the carotid and femoral pulse waveforms. Then, the cfPWV was calculated as 0.8 times the carotid-femoral distance divided by the pulse transit time [5]. For each subject, a representative value was derived from the beat-by-beat cfPWVs by: (1) calculating the average over all beats in each of the two recordings, and (2) taking the mean of these two average values.

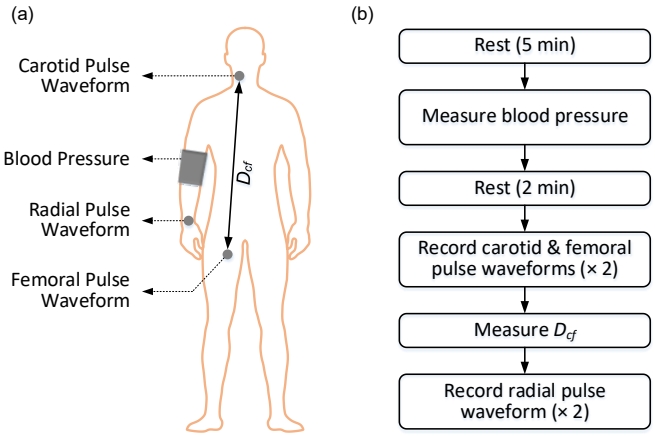

Fig. 1. Experimental details: (a) Signal acquisition; (b) Experimental protocol. D_{cf}: carotid-femoral distance. '×2' means repeated twice.

C. Pulse Wave Analysis

For the two simultaneous measurements in each subject, a series of synthetized aortic pressure waveforms were derived from the SphygmoCor device using the transfer function method [11]. A representative pulse waveform was generated from each time series of the radial and aortic pulse waveforms, by means of the ensemble averaging technique embedded in the device's software. Several features were extracted from the representative radial and aortic pulse waveforms in the time and frequency domains, as well as by applying WSA to the aortic pulse waveforms. See appendix for details.

In the time domain, features were calculated based on the timing and amplitude of several fiducial points (Fig. 2). In the aortic pressure waveform, the timing of the foot indicates the opening of the aortic valve and the start of blood injection. Therefore, the foot corresponds to the diastolic blood pressure in the aorta. The inflection point is associated with wave reflections [16]. The peak marks the highest pressure generated by the heart to drive blood from the central aorta to the

periphery. The notch corresponds to where the aortic valve closes and, in a healthy circulation, when the ejection of blood stops. In the radial pressure waveform, the foot and the notch share the same physiological meaning as in the aortic pressure waveform. The first peak, formed by the aortic forward wave traveling to the radial artery, marks the local systolic blood pressure. The second peak is associated with wave reflections [8]. The diastolic peak has not been sufficiently investigated but was found to provide additive value in estimating cfPWV from the radial pulse waveform in one of our previous studies [17].

The determinations of the foot and notch of the radial and derived aortic pulse waveform were performed using the same method: the foot was determined by the intersecting tangent technique; the notch was identified as the local maximum of the second derivative. For the radial pulse waveform, the first peak was taken as the global maximum. The second peak was identified as the local peak of the measured wave or the local minimum of its second derivative following the first peak. The diastolic peak was identified as the local maximum of the measured wave or the local minimum of its second derivative after the notch. For the derived aortic pulse waveform, the peak was taken as the global maximum. The inflection point was determined as the second peak of the second derivative following the foot, or the local maximum of the second derivative after the peak [18].

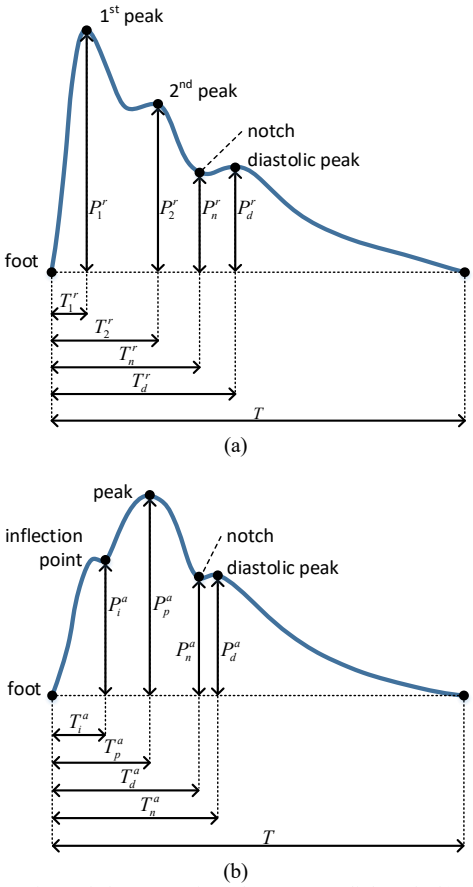

Fig. 2. Extraction of feature points from (a) radial and (b) aortic pulse waveforms.

The timing and amplitude of the first peak, second peak, notch, and diastolic peak with respect to the foot were defined as T_1^r, T_2^r, T_n^r, T_d^r and P_1^r, P_2^r, P_n^r, P_d^r, respectively. The time difference between the first and second peak (T_{12}^r) was calculated as $T_2^r - T_1^r$, which may be associated with aortic stiffness since the first and second peaks are generated mainly by the aortic forward and backward pressure waves from the lower body, respectively. The time ratios $R_{1,n}^{r,T} = T_1^r/T_n^r * 100\%$, $R_{2,n}^{r,T} = \frac{T_2^r}{T_n^r} * 100\%$, as well as $R_n^{r,T} = T_n^r/T * 100\%$, were also calculated. The radial augmentation index and diastolic augmentation index were defined as $AI^r = P_2^r/P_1^r * 100\%$ and $AI_d^r = P_d^r/P_1^r * 100\%$, respectively. The amplitude ratios defined as $R_{n,1}^{r,P} = P_n^r/P_1^r \times 100\%$ and $R_{d,n}^{r,P} = P_d^r/P_n^r \times 100\%$ were also included for feature selection.

Similarly, the timing and amplitude of the peak, inflection point, and notch with respect to the foot of the central aortic pulse waveform were defined as T_p^a, T_i^a, T_n^a and P_p^a, P_i^a, P_n^a, respectively. The time difference between the peak and inflection point was calculated as $T_{p,i}^a = |T_p^a - T_i^a|$, since they are associated with the forward and backward wave, respectively. The diastolic duration was calculated as $T_{dia}^a = T - T_n^a$. Several time ratios were calculated, i.e., $R_{1,n}^{a,T} = T_1^a/T_n^a \times 100\%$, $R_{2,n}^{a,T} = T_2^a/T_n^a \times 100\%$, $R_n^{a,T} = T_n^a/T \times 100\%$, and $R_{dia}^{a,T} = T_{dia}^a/T \times 100\%$. Aortic augmentation index was defined as $(P_p^a - P_i^a)/P_p^a \times 100\%$ if the inflection point appeared before the peak, and $-(P_p^a - P_i^a)/P_p^a \times 100\%$ if the inflection point appeared after the peak. The amplitude ratio between the notch and the peak was calculated ($R_n^{a,P} = P_n^a/P_p^a \times 100\%$), but not between diastolic peak and notch, since a diastolic peak was hardly visible in some subjects. Sub-endocardial variability ratio (SEVR), also known as Buckberg index [19] for assessing subendocardial perfusion, was calculated from the aortic pressure waveform as the area under the curve between the foot and the following notch divided by that between the notch and the following foot.

Frequency-domain features were calculated from the time series of the radial and derived aortic pulse waveforms. After calculation of the frequency spectrum using the fast Fourier transform, the second to the fifth peak amplitudes normalized by the first peak amplitude (H_2^a/H_1^a, H_3^a/H_1^a, H_4^a/H_1^a, and H_5^a/H_1^a for radial pulse waveforms; H_2^r/H_1^r, H_3^r/H_1^r, H_4^r/H_1^r, and H_5^r/H_1^r for aortic pulse waveforms) were included as features in the subsequent analysis, given that the first 5 harmonics of the discrete Fourier series are sufficient to represent most of the variance in radial or aortic pulse waveforms [18].

WSA can be used to assess arterial stiffness because the stiffness of the arteries determines how fast the pulse wave travels along them and the stiffness gradient affects where and to what extent the pulse wave is reflected [20]. Therefore, both the timing and amplitude features from the forward and backward waves are associated with arterial stiffness. WSA based on the aortic pressure waveform alone, as first proposed by Westerhof et al. [21], was applied to the representative

derived aortic pulse waveform. This method approximates the flow waveform by a triangular wave, with duration equal to the ejection duration and peak flow timing equal to that of the inflection point. This 'triangular flow' assumption may sometimes result in large backward wave before the inflection point or sharp forward and backward waves. Following Qasem and Avolio [9], we made a correction by assuming that no reflected wave occurred before the inflection point and maintaining the backward wave amplitude constant from the foot to the inflection point. The time delay (T_{fb}) between the forward and backward wave was calculated by cross-correlation, again following Qasem and Avolio [9]. Reflection magnitude (RM) was calculated as the ratio of the backward wave amplitude to the forward wave amplitude [22]. Reflection index (RI) was calculated as the ratio of the amplitude of the backward wave to the sum of the amplitudes of the forward and backward waves [22]. The determination of the second peak of the radial pulse waveform or the inflection point of the aortic pulse waveform has been shown to be challenging in some subjects. For a more clinically applicable alternative, the timing of peak flow is sometimes determined as 30% of the ejection duration. Both methods were applied in this study. T_{fb30}, RM_{30}, and RI_{30} were T_{fb}, RM, and RI calculated based on this assumption, respectively.

D. Feature Selection and Cross-Validation

Features calculated in the time and frequency domains, as well as from WSA were all considered candidates for cfPWV estimation. Some general information about the subjects was also included. Specifically, the characteristics entered into the feature selection analysis were: gender (G), height (H), weight (W) and body mass index (BMI). As mentioned previously, the clinical significance of cfPWV is its independent and additive value for predicting cardiovascular events over and above conventional risk factors such as age and blood pressure. Thus, age, as well as blood pressure-related features from pulse wave analysis, were not considered in the feature selection. The cardiac period (T), heart rate (HR), calculated as $60/\mathrm{T}$, and pulse pressure ratio between radial and aortic pulse waveform, were also included in the feature selection.

Many of the above calculated features may be related to the pulse transit time (e.g., the timing features and reflection-related features) and their reciprocals, therefore, to pulse wave velocity. As shown in Fig. 3, we generated a set of new features by taking the reciprocal of all the features except for gender, height, cardiac period, and heart rate. Note that we used 1-AI^a instead of AI^a during this procedure, since AI^a may be zero, and its reciprocal could, therefore, go to infinity. Another set of new features was generated by multiplying the above reciprocals by H, assuming that H is positively correlated with pulse transit distance.

The agreement between the two measurements of cfPWV and features from the radial and aortic pulse waveforms was assessed by intra-class correlation (ICC; two-way random effects, absolute agreement, single rater) [23-25]. All features with ICC<0.75 were excluded from subsequent analysis.

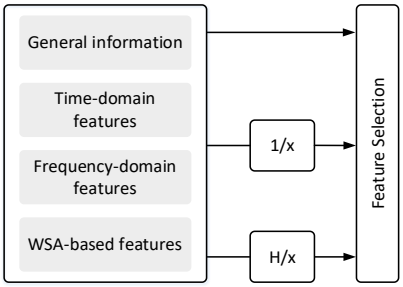

Fig. 3. Feature generation. Three sets of features were included in the selection process: (1) the raw features including subjects' general information and those extracted from time-domain, frequency-domain, and wave separation analysis (WSA); (2) the reciprocal of all the raw features; (3) all the reciprocals multiplied by the body height, H. '1/x' indicates taking the reciprocal. 'H/x' indicates multiplying the height after taking the reciprocal.

The relationship between the features associated with the radial and derived aortic pulse waveforms and cfPWV was investigated through all-possible regressions with bootstrapping. Specifically, every possible combination of the features was entered into a regression model and the ones that better estimated cfPWV (in terms of correlation coefficient) were selected. This process was repeated 100 times by randomly sampling the data with replacement and the correlation coefficients derived were averaged. However, this exhaustive bootstrapping regression becomes computationally expensive as the number of features included in the regression model increases. Therefore, we stopped increasing the number of features to include in the regression models at 4 for all-possible regression analysis, and employed the McHenry's select algorithm, which produces a similar performance with much lower computational cost, as an attempt to include more features in the regression model and improve the estimation performance [26]. Furthermore, linear epsilon-insensitive support vector regression with gaussian kernel was also applied to estimate cfPWV. The hyperparameters were optimized iteratively using Bayesian optimization, with ranges being $[10^{-3}, 10^{3}]$ for the cost, $[10^{-3}, 10^{3}]$ for the kernel scale, and $[10^{-3}, 10^{2}]/1.349$ times the interquartile range of cfPWV for epsilon, where the interquartile range over 1.349 is an estimate of the standard deviation. Each of the selected features/feature pairs was validated via leave-one-out cross-validation. Specifically, the dataset was separated, in all possible ways, into a training set with 110 subjects and a test set with only one subject. A regression model with the selected features was built based on each training set and then applied to the corresponding test set for validation.

E. Numerical Study

The association of pulse wave features with aortic stiffness were further confirmed and investigated using a dataset of simulated pulse waves in thousands of virtual subjects. This dataset was generated by a one-dimensional (1-D) model of blood flow in the 55 larger arterial segments of the human systemic circulation. The cardiac and arterial parameters of the model are listed in Table II, along with their variations, each expressed as a multiple of the baseline value. These variations

of seven basic parameters give a set of 7776 cases, which was reduced to 3325 cases with rejection criteria. Further details can be found in a previous study [27].

TABLE II
BASIC HEMODYNAMIC PARAMETERS AND THE CORRESPONDING MULTIPLICATION FACTORS IN THE COMPUTATIONAL MODEL

Parameters	Symbol/ Abbreviation	Multiplication factor (%)
Elastic arteries PWV	$\boldsymbol{c_e}$	81, 100, 130, 160, 190, 225
Muscular arteries PWV	$\boldsymbol{c_m}$	80, 100, 115, 130
Elastic arteries diameter	$\boldsymbol{D_e}$	90, 100, 120, 140
Muscular arteries diameter	$\boldsymbol{D_m}$	90, 100, 121
Heart rate	HR	85, 100, 115
Stroke volume	SV	80, 100, 120
Peripheral vascular resistance	PVR	90, 100, 110

The definitions of all features in the simulated radial and aortic pulse waves are the same as in the measured pulse waves, while the extraction of the foot and dicrotic notch as well as the wave separation procedure differs. In the measured radial and aortic pulse waves, the foot was extracted via the intersecting tangent method. In the numerical study, the foot of the radial and aortic pulse waveform was simply defined as the local minimum in late diastole. The dicrotic notch was defined as the point 0.31s after the foot, due to the fact that the ejection period was set to 0.31s. Furthermore, wave separation was applied to the aortic pulse waveform based on the model-generated flow waves instead of the triangular approximation used for the in vivo data, along with the local pulse wave velocity [28]. The forward (P_f) and backward (P_b) pressure waveform can be calculated using the following equations,

$$dP_f = \frac{1}{2}(dP + \rho c dU) \quad (1)$$

$$dP_b = \frac{1}{2}(dP - \rho c dU) \quad (2)$$

where ρ is the blood density, and c represents the pulse wave velocity.

Local sensitivity analysis was employed to quantify the association of $R_{n,d}^{r,P}$ with aortic PWV (as measured by c_e), as well as other hemodynamic parameters (c_m, D_e, D_m, HR, SV, PVR) in 1-D model. As a comparison, the effect of the hemodynamic parameters on cfPWV, RM, and T_{fb} was also analyzed using local sensitivity analysis.

The sensitivity of a pulse wave feature y to a basic hemodynamic parameter x was defined as

$$I_i(x_1, \cdots, x_n) = \frac{\Delta y}{y_{max} - y_{min}} \frac{x_{max} - x_{min}}{\Delta x_i} \quad (3)$$

where Δy means the change in y due to the change in x_i when other basic hemodynamic parameters x_j ($j \neq i$) remain constant. The subscripts 'max' and 'min' indicate global maximum and minimum across the dataset, respectively.

Most of the pulse wave features that correlate with aortic stiffness are associated with pulse wave reflection. Therefore, we went a step further to investigate the relationship between wave reflection and the association between $R_{n,d}^{r,P}$ and aortic stiffness. The amplitude ratio between the diastolic peak and the notch from both the whole radial pulse waveform (i.e., $R_{n,d}^{r,P}$) and its corresponding forward pulse waveform (denoted as $R_{n,d}^{rf,P}$) was calculated. A comparison between the sensitivity of $R_{n,d}^{r,P}$ and $R_{n,d}^{rf,P}$ versus the hemodynamic parameters of the 1-D model was applied. Additionally, the correlation coefficient between $R_{n,d}^{r,P}$ and $R_{n,d}^{rf,P}$ was calculated. If the association of $R_{n,d}^{r,P}$ with aortic stiffness is dependent on wave reflection, the sensitivity of $R_{n,d}^{rf,P}$ should not follow that of $R_{n,d}^{r,P}$ and the correlation between the two should be poor. The same definition (deriving $R_{n,d}^{a,P}$ and $R_{n,d}^{af,P}$) and analysis was applied to the aortic pressure wave, as a comparison for $R_{n,d}^{r,P}$ and $R_{n,d}^{rf,P}$.

III. RESULTS

The HR difference between the measurements derived from carotid/femoral and radial pulse waveforms was: -1±4 bpm. The difference between the two repeated measurements of cfPWV was 0±0.3 m/s, and the ICC was 0.99. In the ICC analysis, 62/127 of the features gave an ICC of ≥ 0.9; 28/127 gave an ICC of ≥ 0.75; and 31/127, ≥ 0.5. 6/127 of the features gave ICC values < 0.5. These were: $R_{2,1}^{r,H}$, $1/R_{n,1}^{r,P}$, $1/R_{2,1}^{r,H}$, $H/R_{n,1}^{r,P}$, $H/R_{2,1}^{r,H}$, $R_{d,n}^{r,P}$. Thus, 90/127 features were included for feature selection, these being the ones giving ICC values ≥ 0.75.

Including N=1 to 4 features in the regression model gave correlation coefficients of r=0.70±0.02, r=0.77±0.02, r=0.81±0.02, and r=0.82±0.02, respectively. The top 5 features/feature pairs for the univariate (N=1) and the bivariate (N=2) regression models are listed in Table III, along with the corresponding correlation coefficients. The conventional AIx (AI^a and AI^r) positively correlated with cfPWV, both with r=0.60±0.04 (not listed in the table). The correlation coefficients between the measured and estimated cfPWV in cross validation were r=0.68, r=0.75, r=0.79, and r=0.81, for the best feature/feature pairs when N=1 to 4, respectively. Fig. 4 shows the cross-validation result for the best regression model with N=4 independent variables. The estimation errors were 0±1.3, 0±1.2, 0±1.1, and 0±1.1 m/s for N=1 to 4, respectively.

TABLE III
FEATURE SELECTION: TOP 5 REGRESSION MODELS WITH N=1-2 INDEPENDENT VARIABLES

Ranking	N=1		N=2	
	Feature	*r*	*Features*	*r*
1	$\boldsymbol{H/T_{fb}}$	0.70 ±0.02	$\boldsymbol{1/T_{fb}; G}$	0.77±0.02
2	$\boldsymbol{1/T_{fb}}$	0.69±0.02	$\boldsymbol{AI_d^r; RM}$	0.75±0.02
3	$\boldsymbol{R_{n,d}^{r,P}}$	0.67±0.03	$\boldsymbol{1/T_d^r; HR_{n,d}^{r,P}}$	0.74±0.03
4	$\boldsymbol{RI_{30}}$	0.67±0.03	$\boldsymbol{AI_d^r; RM_{30}}$	0.74±0.03
5	$\boldsymbol{HR_{n,d}^{r,P}}$	0.66±0.03	$\boldsymbol{AI_d^r; RI}$	0.74±0.02

Superscripts 'a' and 'r' denote features from the aortic and radial pulse waveforms, respectively; N: number of independent variables in the regression model; r: correlation coefficient; $R_{n,d}^{r,P}$ is the reciprocal of $R_{d,n}^{r,P}$. This notation is used hereafter.

Fig. 5 shows the correlation coefficients between the measured and the estimated cfPWV from features (N=1-20) selected using the McHenry's select algorithm during cross-validation. Fig. 6 is a comparison of the measured and the estimated cfPWV when N=10 features were selected via

McHenry's select algorithm during cross-validation. Fig. 7 shows a comparison of the measured and estimated cfPWV by support vector regression during cross-validation.

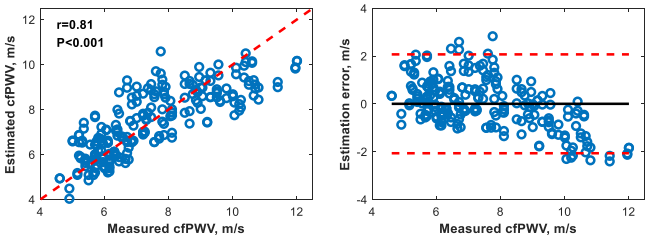

(a) (b)

Fig. 4. Cross-validation of the best feature combination selected when including N=4 features in the regression model. (a) scatter plots of measured versus estimated carotid-femoral pulse wave velocity; (b) Bland-Altman plot of the measured versus estimated carotid-femoral pulse wave velocity.

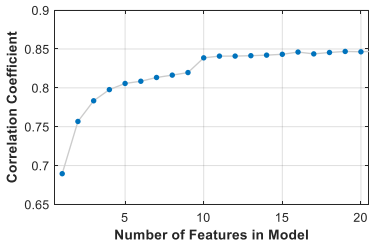

Fig. 5. Cross-validation of the features selected via McHenry's select algorithm: correlation coefficients between estimated and measured cfPWV when the number of features k ranges from 1 to 20.

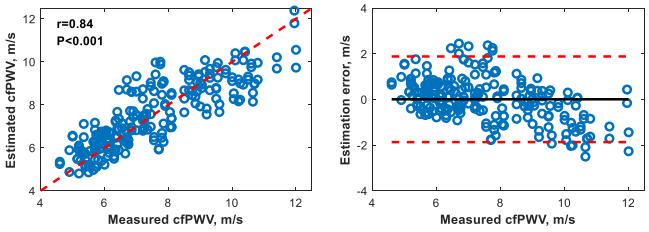

(a) (b)

Fig. 6. Cross-validation of the features selected via McHenry's select algorithm with N=10 features included in the regression model. (a) scatter plots of measured versus estimated carotid-femoral pulse wave velocity; (b) Bland-Altman plot of the measured versus estimated carotid-femoral pulse wave velocity.

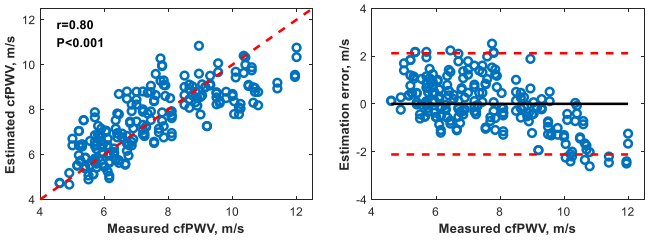

(a) (b)

Fig. 7. Cross-validation of the support vector regression method for the estimation of carotid-femoral pulse wave velocity. (a) scatter plots of measured versus estimated carotid-femoral pulse wave velocity; (b) Bland-Altman plot of the measured versus estimated carotid-femoral pulse wave velocity.

Fig. 8 shows the sensitivity of cfPWV, RM, T_{fb} and $R_{n,d}^{r,P}$ versus several basic hemodynamic parameters. Each blue bar represents the mean sensitivity value of a pulse wave feature (or cfPWV) for one of the basic hemodynamic parameters. The error bars are $\pm$ SD. Fig. 9 presents spider plots of cfPWV, RM, T_{fb} and $R_{n,d}^{r,P}$, when all multiplication factors for the basic hemodynamic parameters of the 1-D model are set equal to 100%. Each line indicates the change of a pulse wave feature (or cfPWV) with one of the basic hemodynamic parameters when the others are kept constant (i.e., multiplication factors equal 100%). Similarly, Fig. 10 shows the sensitivity comparison of $R_{n,d}^{r,P}$, $R_{n,d}^{rf,P}$, $R_{n,d}^{a,P}$ and $R_{n,d}^{af,P}$ versus basic hemodynamic model parameters. Fig. 11 presents spider plots of $R_{n,d}^{r,P}$, $R_{n,d}^{rf,P}$, $R_{n,d}^{a,P}$ and $R_{n,d}^{af,P}$, when all multiplication factors for the basic hemodynamic parameters of the 1-D model equal 100%. Fig. 12 presents the correlation analysis between $R_{n,d}^{r,P}$ and $R_{n,d}^{rf,P}$.

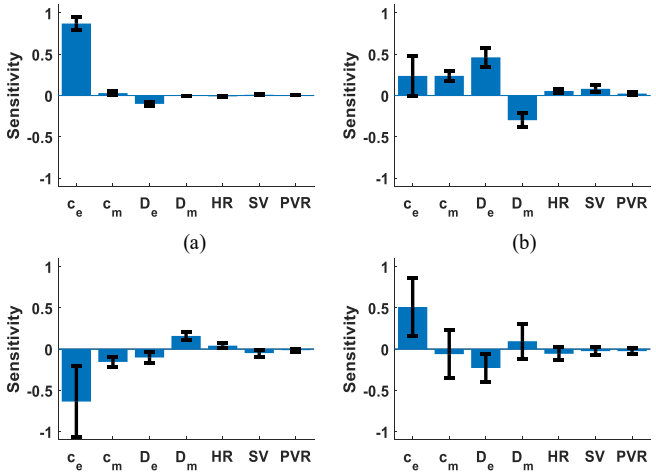

(a) (b) (c) (d)

Fig. 8. Sensitivity analysis of pulse wave features versus some of the basic hemodynamic model parameters: (a) cfPWV; (b) RM; (c) T_{fb}; (d) $R_{n,d}^{r,P}$.

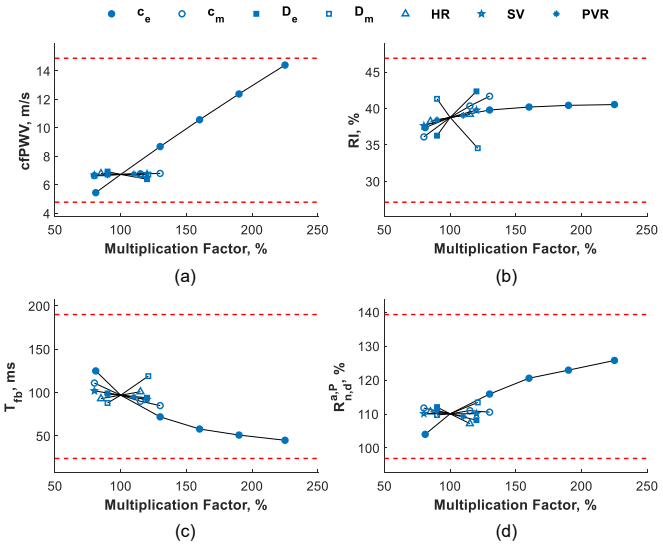

(a) (b) (c) (d)

Fig. 9. Spider plot analysis on pulse wave features when the multiplication factors for all the basic hemodynamic parameters of the 1-D model were equal to 100%: (a) cfPWV; (b) RM; (c) T_{fb}; (d) $R_{n,d}^{r,P}$. Red dashed lines: range of pulse wave features.

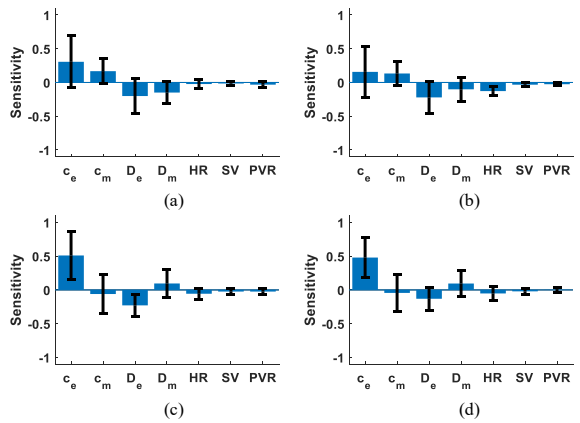

Fig. 10. Sensitivity analysis of $R_{n,d}^{P}$ calculated from different pulse waves versus all basic hemodynamic 1-D model parameters: (a) $R_{n,d}^{a,P}$; (b) $R_{n,d}^{af,P}$; (c) $R_{n,d}^{r,P}$; (d) $R_{n,d}^{rf,P}$.

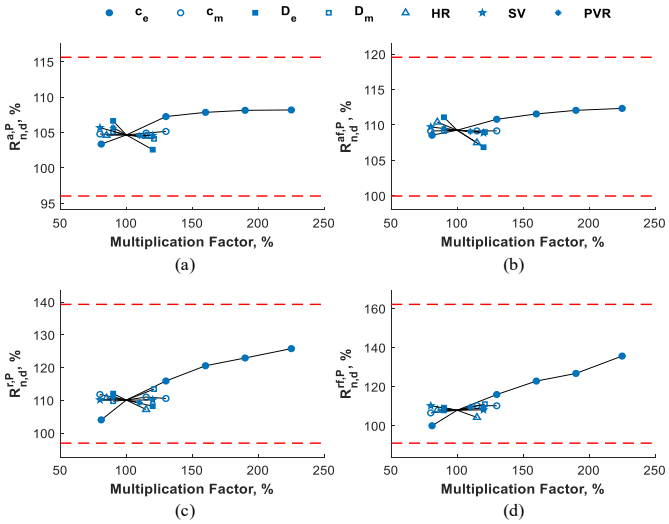

Fig. 11. Spider plot analysis of the amplitude ratio between the diastolic peak and the notch calculated from different pulse waves versus basic hemodynamic model parameters: (a) aortic pulse wave ($R_{n,d}^{a,P}$); (b) aortic forward wave ($R_{n,d}^{af,P}$); (c) radial pulse wave ($R_{n,d}^{r,P}$); (d) radial forward wave ($R_{n,d}^{rf,P}$). Red dashed lines: range of pulse wave features.

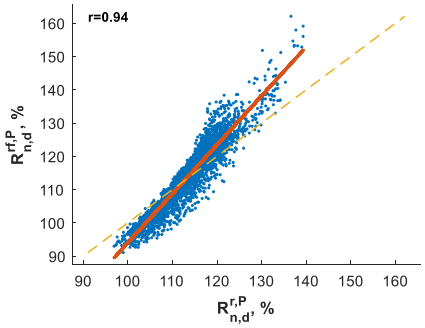

Fig. 12. Scatter plot and correlation analysis of the amplitude ratio between the diastolic peak and the notch calculated from the radial pulse wave and forward wave. Red solid line: regression between $R_{n,d}^{r,P}$ and $R_{n,d}^{rf,P}$. Orange dashed line: $R_{n,d}^{r,P}$=$R_{n,d}^{rf,P}$.

IV. Discussion

This study has identified features/feature pairs that can estimate cfPWV more accurately than single feature-based approaches, which estimate cfPWV from the augmentation index or one of the wave separation features.

A. Validity of the Experimental Data

The reliability of the cfPWV measurement is substantiated by the fact that: (1) the cardiovascular status of the subjects did not change much during the two measurements (HR change: -1±4 bpm); (2) the repeated measurements of cfPWV were close (difference: 0±0.3 m/s; ICC=0.99). The derived radial pulse waveform was validated by a signal quality index embedded in the SphygmoCor device. Most of the pulse wave features showed good repeatability (121/127 of them yielded ICC values of $\geq$ 0.5). Poor agreement (ICC<0.5) between the two measurements was found only in the remaining 6/127 features. Possible reasons are: (1) some of the feature points (e.g., the second peak of the radial pulse waveform) were hard to extract reliably from the waveforms in some subjects (e.g., $R_{2,1}^{r,H}$, $1/R_{2,1}^{r,H}$, $H/R_{2,1}^{r,H}$); (2) multiplying and/or reciprocal operations enlarged the difference between measurements (e.g., $1/R_{n,1}^{r,P}$, $H/R_{n,1}^{r,P}$, $R_{d,n}^{r,P}$). These features should be avoided in clinical assessment of arterial stiffness, even if they are physiologically relevant. In this paper, as mentioned above, only features with ICC>0.75 (n=90) were included in the subsequent analysis.

B. Physiological Relevance of the Selected Features

The features selected in the univariate regression analysis were interpretable and corresponded well with the findings in previous studies [8, 9]. WSA-related timing features H/T_{fb} and $1/T_{fb}$ correlated best with cfPWV (r=0.70 and r=0.69, respectively). A plausible explanation is that T_{fb}, which represents the time for the pressure wave to travel from the aorta to the lower body and back, is, to a large extent, determined by the stiffness of the artery through which the pressure wave passes (e.g., thoracic and abdominal aorta), as well as their combined length [29, 30]. This supports the findings of Qasem and Avolio [9] and also the recommendation from the statement of the American Heart Association [6] that WSA should be applied when assessing wave reflection. WSA-related amplitude features, which represent the magnitude of the reflected wave, also correlated well with cfPWV (e.g., RI_{30} with r=0.67). This may be attributed to the fact that an increase in central arterial stiffness, for instance due to ageing, cancels out the stiffness mismatch between the central and peripheral arteries, thereby lowering wave reflection [20]. The selection of $R_{n,d}^{r,P}$ (r=0.67) is interesting since its correlation with cfPWV is, to the best of our knowledge, reported for the first time, and little work has been done on understanding its physiological basis or the diastolic peak of the radial pulse wave. Furthermore, this feature is not associated with the second peak of the radial pulse, which makes it easy to extract automatically.

In the numerical study, the high sensitivity of cfPWV versus aortic PWV (Fig. 8) confirms the feasibility of using cfPWV as a surrogate for aortic PWV. Other hemodynamic parameters showed hardly any effect on cfPWV. The change of aortic PWV

alone caused the variation (almost linearly) of cfPWV over almost its full range. The sensitivity of T_{fb} versus aortic PWV was also found to be much higher than versus any other basic hemodynamic parameters. RM is affected by aortic PWV, but also by other hemodynamic parameters (c_m, D_e and D_m). The effect of aortic PWV on $R_{n,d}^{r,P}$ is much larger than any other hemodynamic parameters. The same can be seen from the spider plots (Fig. 9). These results agree well with the association of parameters $R_{n,d}^{r,P}$, T_{fb} and RM with cfPWV found in the measured data.

The sensitivity of $R_{n,d}^{r,P}$ versus aortic PWV was higher than that of $R_{n,d}^{a,P}$ (Fig. 10 and Fig. 11), in agreement with the observation that $R_{n,d}^{r,P}$ was more closely associated with cfPWV in the analysis of the measured data. The effect of all the basic hemodynamic parameters on $R_{n,d}^{r,P}$ and $R_{n,d}^{rf,P}$ was similar. Additionally, $R_{n,d}^{r,P}$ and $R_{n,d}^{rf,P}$ were closely correlated (r=0.94; Fig. 12), showing that the amplitude ratio of the diastolic peak and dicrotic notch are not affected by wave reflection.

Multiplying the reciprocals by the height of the body (H) did not result in much improvement in the correlation with cfPWV. Indeed, in univariate regression analysis, H/T_{fb} outperformed $1/T_{fb}$ in terms of correlation coefficient by only 0.1, and $HR_{n,d}^{r,P}$ failed to outperform $R_{n,d}^{r,P}$ (Table III). This suggests that H may not be, or only modestly be, associated with the effective reflection distance. Using the carotid-femoral distance instead of H may not improve the correlation coefficient. Indeed, when using this variable instead of H, the correlation coefficients were r=0.69±0.02, r=0.77±0.02, r=0.81±0.02 and r=0.82±0.02, for N=1 to 4, respectively, whereas the corresponding values for H were r=0.70±0.02, r=0.77±0.02, r=0.81±0.02, and r=0.82±0.02, respectively.

C. Potential of Radial Pulse Waveform to Estimate cfPWV

In cross-validation, the regression models showed satisfactory results (r=0.68, r=0.75, r=0.79, and r=0.81; estimation error: 0±1.3, 0±1.2, 0±1.1, and 0±1.1 m/s for N= 1 to 5; Fig. 4). These correlation coefficients are close to those in the feature selection results (Table III), which demonstrate that the regression analysis in this study does not suffer from over-fitting. McHenry's select algorithm and support vector regression also produced pleasing results (r=0.84 and r=0.80, respectively). Therefore, we may conclude that the radial pulse waveform alone has the potential to estimate cfPWV.

Increasing the number of features included in the regression model may further improve the estimation of cfPWV. During cross-validation, the correlation coefficient between the measured and the estimated cfPWV from features selected via McHenry's select algorithm was improved from 0.8 (when including N=4 features) to 0.84, although at the cost of including more features in the model (in this case 10).

An inverse relationship (r=-0.49, p<0.001 for McHenry's select algorithm when N=10 and r=-0.59, p<0.001 for support vector regression) between the estimation error and the measured value of cfPWV was found (Fig. 6 and 7, right). This may be attributed to the nonlinearity of the relation between cfPWV and the features derived from pulse wave analysis. Future work is required and may potentially further improve the estimation of cfPWV.

D. Considerations for Applicability and Reliability

One of the main drawbacks of the conventional AIx and the WSA technique applied in previous studies, for instance [9], is that the second peak of the radial pulse waveform or the inflection point of the aortic pulse waveform is hard to determine in some subjects. This could be addressed by the feature pairs in Table III, which do not consider those points. In the univariate regression analysis, RI_{30}, $R_{n,d}^{r,P}$ and $HR_{n,d}^{r,P}$ were neither associated with the second peak of the radial pulse waveform, nor the inflection point of the aortic pulse waveform. In bivariate regression analysis, the feature pairs $1/T_d^r$ and $HR_{n,d}^{r,P}$, as well as AI_d^r and RM_{30}, do not rely on those hard-to-determine feature points. Therefore, cfPWV may be estimated without having to deal with the difficulty of finding the second peak of the radial pulse waveform or the inflection point of the aortic pulse waveform.

V. Conclusion

This study has demonstrated that (1) cfPWV can be estimated more accurately from the selected features/feature pairs of the radial and derived aortic pulse waveforms; (2) the features/feature pairs selected are physiologically interpretable; (3) some of the selected features/feature pairs are not associated with the sometimes poorly defined second peak of the radial waveform or the inflection point of the aortic waveform, and may therefore serve as more reliable and accurate substitutes for the conventional pulse wave analysis approach; (4) the ratio of the diastolic peak amplitude to the notch amplitude of the radial pulse waveform is a potential feature for cfPWV estimation and arterial stiffness assessment that is independent of wave reflections.

Acknowledgment

The authors declare no conflict of interest.

References

[1] C. Vlachopoulos, K. Aznaouridis, and C. Stefanadis, "Prediction of cardiovascular events and all-cause mortality with arterial stiffness: a systematic review and meta-analysis," *Journal of the American College of Cardiology,* vol. 55, no. 13, pp. 1318-1327, 2010.

[2] Y. Ben-Shlomo, M. Spears, C. Boustred, M. May, S. G. Anderson, E. J. Benjamin, P. Boutouyrie, J. Cameron, C. H. Chen, J. K. Cruickshank, S. J. Hwang, E. G. Lakatta, S. Laurent, J. Maldonado, G. F. Mitchell, S. S. Najjar, A. B. Newman, M. Ohishi, B. Pannier, T. Pereira, R. S. Vasan, T. Shokawa, K. Sutton-Tyrell, F. Verbeke, K. L. Wang, D. J. Webb, T. Willum Hansen, S. Zoungas, C. M. McEniery, J. R. Cockcroft, and I. B. Wilkinson, "Aortic pulse wave velocity improves cardiovascular event prediction: an individual participant meta-analysis of prospective observational data from 17,635 subjects," *Journal of the American College of Cardiology,* vol. 63, no. 7, pp. 636-646, Feb 25, 2014.

[3] F. Mitchell Gary, S.-J. Hwang, S. Vasan Ramachandran, G. Larson Martin, J. Pencina Michael, M. Hamburg Naomi, A. Vita Joseph, D. Levy,

and J. Benjamin Emelia, "Arterial stiffness and cardiovascular events: the Framingham Heart Study," *Circulation,* vol. 121, no. 4, pp. 505-511, 2010/02/02, 2010.

[4] S. Laurent, J. Cockcroft, L. Van Bortel, P. Boutouyrie, C. Giannattasio, D. Hayoz, B. Pannier, C. Vlachopoulos, I. Wilkinson, H. Struijker-Boudier, and A. European Network for Non-invasive Investigation of Large, "Expert consensus document on arterial stiffness: methodological issues and clinical applications," *European Heart Journal,* vol. 27, no. 21, pp. 2588-605, Nov, 2006.

[5] L. M. Van Bortel, S. Laurent, P. Boutouyrie, P. Chowienczyk, J. Cruickshank, T. De Backer, J. Filipovsky, S. Huybrechts, F. U. Mattace-Raso, and A. D. Protogerou, "Expert consensus document on the measurement of aortic stiffness in daily practice using carotid-femoral pulse wave velocity," *Journal of Hypertension,* vol. 30, no. 3, pp. 445-448, 2012.

[6] R. R. Townsend, I. B. Wilkinson, E. L. Schiffrin, A. P. Avolio, J. A. Chirinos, J. R. Cockcroft, K. S. Heffernan, E. G. Lakatta, C. M. McEniery, and G. F. Mitchell, "Recommendations for improving and standardizing vascular research on arterial stiffness: a scientific statement from the American Heart Association," *Hypertension,* vol. 66, no. 3, pp. 698-722, 2015.

[7] B. Williams, G. Mancia, W. Spiering, E. Agabiti Rosei, M. Azizi, M. Burnier, D. L. Clement, A. Coca, G. De Simone, and A. Dominiczak, "2018 ESC/ESH Guidelines for the management of arterial hypertension," *European Heart Journal,* vol. 39, no. 33, pp. 3021-3104, 2018.

[8] W. W. Nichols, "Clinical measurement of arterial stiffness obtained from noninvasive pressure waveforms," *American Journal of Hypertension,* vol. 18, no. 1 Pt 2, pp. 3s-10s, Jan, 2005.

[9] A. Qasem, and A. Avolio, "Determination of aortic pulse wave velocity from waveform decomposition of the central aortic pressure pulse," *Hypertension,* vol. 51, no. 2, pp. 188-195, 2008/02/01, 2008.

[10] S. S. Hickson, W. W. Nichols, Yasmin, B. J. McDonnell, J. R. Cockcroft, I. B. Wilkinson, C. M. McEniery, and A. S. I. on behalf of the, "Influence of the central-to-peripheral arterial stiffness gradient on the timing and amplitude of wave reflections," *Hypertension Research,* vol. 39, no. 10, pp. 723-729, 2016/10/01, 2016.

[11] C.-H. Chen, E. Nevo, B. Fetics, P. H. Pak, F. C. Yin, W. L. Maughan, and D. A. Kass, "Estimation of central aortic pressure waveform by mathematical transformation of radial tonometry pressure," *Circulation,* vol. 95, no. 7, pp. 1827-1836, 1997.

[12] S. Mallat, *A wavelet tour of signal processing*: Academic press, 1999.

[13] L. Xu, D. Zhang, and K. Wang, "Wavelet-based cascaded adaptive filter for removing baseline drift in pulse waveforms," *IEEE Transactions on Biomedical Engineering,* vol. 52, no. 11, pp. 1973-1975, 2005.

[14] R. Mukkamala, J.-O. Hahn, O. T. Inan, L. K. Mestha, C.-S. Kim, H. Töreyin, and S. Kyal, "Toward ubiquitous blood pressure monitoring via pulse transit time: theory and practice," *IEEE Transactions on Biomedical Engineering,* vol. 62, no. 8, pp. 1879-1901, 2015.

[15] G. Zhang, M. Gao, D. Xu, N. B. Olivier, and R. Mukkamala, "Pulse arrival time is not an adequate surrogate for pulse transit time as a marker of blood pressure," *Journal of Applied Physiology,* vol. 111, no. 6, pp. 1681-1686, 2011.

[16] M. F. O'Rourke, and T. Yaginuma, "Wave Reflections and the Arterial Pulse," *Archives of Internal Medicine,* vol. 144, no. 2, pp. 366-371, 1984.

[17] Y. Yao, L. Hao, L. Xu, Y. Zhang, L. Qi, Y. Sun, B. Yang, F. N. van de Vosse, and Y. Yao, "Diastolic augmentation index improves radial augmentation index in assessing arterial stiffness," *Scientific Reports,* vol. 7, no. 1, pp. 5864, 2017.

[18] W. Nichols, M. O'Rourke, and C. Vlachopoulos, *McDonald's Blood Flow in Arteries: Theoretical, Experimental and Clinical Principles*: CRC press, 2011.

[19] G. D. Buckberg, D. E. Fixler, J. P. Archie, and J. I. Hoffman, "Experimental subendocardial ischemia in dogs with normal coronary arteries," *Circulation research,* vol. 30, no. 1, pp. 67-81, 1972.

[20] S. Greenwald, A. Carter, and C. Berry, "Effect of age on the in vitro reflection coefficient of the aortoiliac bifurcation in humans," *Circulation,* vol. 82, no. 1, pp. 114-123, 1990.

[21] E. Westerhof Berend, I. Guelen, N. Westerhof, M. Karemaker John, and A. Avolio, "Quantification of wave reflection in the human aorta from pressure alone," *Hypertension,* vol. 48, no. 4, pp. 595-601, 2006/10/01, 2006.

[22] N. Westerhof, N. Stergiopulos, M. I. M. Noble, and B. E. Westerhof, "Wave Separation and Waveform Analysis," *Snapshots of Hemodynamics: An Aid for Clinical Research and Graduate Education*, N. Westerhof, N. Stergiopulos, M. I. M. Noble and B. E. Westerhof, eds., pp. 175-183, Cham: Springer International Publishing, 2019.

[23] K. O. McGraw, and S. P. Wong, "Forming inferences about some intraclass correlation coefficients," *Psychological Methods,* vol. 1, no. 1, pp. 30, 1996.

[24] P. E. Shrout, and J. L. Fleiss, "Intraclass correlations: uses in assessing rater reliability," *Psychological Bulletin,* vol. 86, no. 2, pp. 420, 1979.

[25] D. Liljequist, B. Elfving, and K. Skavberg Roaldsen, "Intraclass correlation – A discussion and demonstration of basic features," *PLoS one,* vol. 14, no. 7, pp. e0219854, 2019.

[26] C. E. McHenry, "Computation of a best subset in multivariate analysis," *Journal of the Royal Statistical Society: Series C (Applied Statistics),* vol. 27, no. 3, pp. 291-296, 1978.

[27] M. Willemet, P. Chowienczyk, and J. Alastruey, "A database of virtual healthy subjects to assess the accuracy of foot-to-foot pulse wave velocities for estimation of aortic stiffness," *American Journal of Physiology-Heart and Circulatory Physiology,* vol. 309, no. 4, pp. H663-H675, 2015.

[28] K. H. Parker, and C. Jones, "Forward and backward running waves in the arteries: analysis using the method of characteristics," *Journal of Biomechanical Engineering-Transactions of the ASME,* vol. 112, 1990.

[29] A. I. Moens, *Die Pulskurve*, Leiden, The Netherlands: E.J. Brill., 1878.

[30] D. Korteweg, "Ueber die Fortpflanzungsgeschwindigkeit des Schalles in elastischen Röhren," *Annalen der Physik,* vol. 241, no. 12, pp. 525-542, 1878.

APPENDIX

In this study, three sets of features were included in feature selection: (1) the raw features including subjects' general information and those extracted from time-domain, frequency-domain, and wave separation analysis; (2) the reciprocal of all the raw features; (3) all the reciprocals multiplied by body height. This appendix is a full list of all the raw features (Table Appendix I). The 2nd and 3rd sets of features can be easily obtained from the raw features, except gender, height, cardiac cycle, and heart rate, by taking the reciprocals, and multiplying the reciprocals by body height.

TABLE APPENDIX I

A LIST OF FEATURES EXTRACTED FOR THE ESTIMATION OF CENTRAL PULSE WAVE VELOCITY, ALONG WITH THE DEMOGRAPHICS. NOTE THAT THE FEATURES GENDER, HEIGHT, T, AND HEART RATE (HR) WERE NOT INCLUDED WHEN GENERATING NEW FEATURES BY TAKING THE RECIPROCAL (AND SCALING BY HEIGHT; SEE BELOW). ALSO, WE USED 1-AI^A INSTEAD OF AI^A DURING THIS PROCESS. SEVR, BUCKBERG SUB-ENDOCARDIAL VIABILITY RATIO. RM: REFLECTION MAGNITUDE. RI: REFLECTION INDEX.

Categories	Features	Definition/calculation
General information	G #	Gender
	H #	Height
	W	Weight
	BMI	Body mass index
	T #	Cardiac cycle
	HR #	Heart rate: $60/T$
	$R_{PP}^{r,a}$	Ratio between radial and aortic pulse pressure
Time-domain features of radial pulse waveform	T_1^r	Time to the first peak
	T_2^r	Time to the second peak
	T_n^r	Time to the notch (ejection duration)
	T_d^r	Time to the diastolic peak
	T_{12}^r	$T_2^r - T_1^r$
	$R_{1,n}^{r,T}$	$T_1^r/T_n^r \times 100\%$
	$R_{2,n}^{r,T}$	$T_2^r/T_n^r \times 100\%$
	$R_n^{r,T}$	$T_n^r/T \times 100\%$
	AI^r	Radial augmentation index: $P_2^r/P_1^r \times 100\%$
	AI_d^r	$P_d^r/P_1^r \times 100\%$
	$R_{n,1}^{r,P}$	$P_n^r/P_1^r \times 100\%$
	$R_{d,n}^{r,P}$	$P_d^r/P_n^r \times 100\%$
Time-domain features of aortic pulse waveform	T_p^a	Time to the peak
	T_i^a	Time to the inflection point
	T_n^a	Time to the notch (ejection duration)
	$T_{p,i}^a$	$\left\|T_p^a - T_i^a\right\|$
	T_{dia}^a	Diastolic duration: $T - T_n^a$
	$R_{1,n}^{a,T}$	$T_1^a/T_n^a \times 100\%$
	$R_{2,n}^{a,T}$	$T_2^a/T_n^a \times 100\%$
	$R_n^{a,T}$	$T_n^a/T \times 100\%$
	$R_{dia}^{a,T}$	$T_{dia}^a/T \times 100\%$
	AI^a	Augmentation index: • $(P_p^a - P_i^a)/P_p^a \times 100\%$ if inflection point appears before the peak; • $-(P_p^a - P_i^a)/P_p^a \times 100\%$ if inflection point appears after the peak.
	$R_n^{a,P}$	$P_n^a/P_p^a \times 100\%$
	$SEVR$	Ratio of the area under the pressure waveform in systolic and diastolic period
Frequency-domain features of radial pulse waveform	$R_{2,1}^{r,H}$	$H_2^r/H_1^r \times 100\%$
	$R_{3,1}^{r,H}$	$H_3^r/H_1^r \times 100\%$
	$R_{4,1}^{r,H}$	$H_4^r/H_1^r \times 100\%$
	$R_{5,1}^{r,H}$	$H_5^r/H_1^r \times 100\%$
Frequency-domain features of aortic pulse waveform	$R_{2,1}^{a,H}$	$H_2^a/H_1^a \times 100\%$
	$R_{3,1}^{a,H}$	$H_3^a/H_1^a \times 100\%$
	$R_{4,1}^{a,H}$	$H_4^a/H_1^a \times 100\%$
	$R_{5,1}^{a,H}$	$H_5^a/H_1^a \times 100\%$
Wave separation features	T_{fb}	Delay between the forward and backward wave
	T_{fb30}	Delay between the forward and backward wave (using 30%T_n^a as an approximate of T_i^a)
	RI	Ratio of the backward wave amplitude to the sum of forward and backward wave amplitude
	RI_{30}	Ratio of the backward wave amplitude to the sum of forward and backward wave amplitude (using 30%T_n^a as an approximate of T_i^a)
	RM	Amplitude ratio of backward wave to the forward wave
	RM_{30}	Amplitude ratio of backward wave to the forward wave (using 30%T_n^a as an approximate of T_i^a)

Superscripts 'a' and 'r' denote features from the aortic and radial pulse waveforms, respectively;
#: these features were not included when taking the reciprocal or multiplying the reciprocal by body height.